DNA Self-Assembly Mediated by Programmable Soft-Patchy Interactions

Sanja Novak,[†] Jing Zhang,[*,†,#] Emmanuel Kentzinger,[‡] Ulrich Rücker,[‡] Giuseppe Portale,[*,¶] Niklas Jung,[§] Ulrich Jonas,[§] Jin S. Myung,[∥,@] Roland G. Winkler,[∥] Gerhard Gompper,[∥] Jan K. G. Dhont,[†,⊥] and Emmanuel Stiakakis[*,†]

†*Biomacromolecular Systems and Processes, Institute of Biological Information Processing (IBI-4), Forschungszentrum Jülich, D-52425 Jülich, Germany*
‡*Jülich Centre for Neutron Science JCNS and Peter Grünberg Institut PGI, JARA-FIT, Forschungszentrum Jülich, D-52425 Jülich, Germany*
¶*Univ Groningen, Zernike Inst. Adv. Mat. Macromol Chem & New Polymer Mat, NL-9747 AG Groningen, Netherlands*
§*Macromolecular Chemistry, Department Chemistry-Biology, University of Siegen, D-57076 Siegen, Germany*
∥*Theoretical Physics of Living Matter, Institute of Biological Information Processing (IBI-5) and Institute for Advanced Simulation (IAS-2), Forschungszentrum Jülich, D-52425 Jülich, Germany*
⊥*Heinrich-Heine-Universität Düsseldorf, D-40225 Düsseldorf, Germany*
#*Current address: Department of Environmental Nano-materials, Research Center for Eco-Environmental Sciences, Chinese Academy of Sciences, Beijing 100085, China*
@*Current address: Chemical Materials Solutions Center, Korea Research Institute of Chemical Technology, Daejeon 34114, Korea*

E-mail: jingzhang@rcees.ac.cn; g.portale@rug.nl; e.stiakakis@fz-juelich.de

Abstract

Adding shape and interaction anisotropy to a colloidal particle offers exquisitely tunable routes to engineer a rich assortment of complex-architected structures. Inspired by the hierarchical self-assembly concept with block copolymers and DNA liquid crystals, and exploiting the unique assembly properties of DNA, we report here the construction and self-assembly of DNA-based soft-patchy anisotropic particles with a high degree of modularity in the system's design. By programmable positioning of thermo-responsive polymeric patches on the backbone of a stiff DNA duplex with linear and star-shaped architecture, we reversibly drive the DNA from a disordered ensemble to a diverse array of long-range ordered multidimensional nanostructures with tunable lattice spacing, ranging from lamellar to bicontinuous double-gyroid and double-diamond cubic morphologies, through the alteration of temperature. Our results demonstrate that the proposed hierarchical self-assembly strategy can be applied to any kind of DNA nanoarchitecture, highlighting the design principles for integration of self-assembly concepts from the physics of liquid crystals, block copolymers and patchy colloids into the continuously growing interdisciplinary research field of structural DNA nanotechnology.

Keywords

DNA, self-assembly, anisotropic patchy particles, liquid crystals, block copolymers.

One of the most well-established bottom-up self-assembly strategies in soft matter for achieving exquisitely complex and long-range order in one, two, and three dimensions (1D, 2D and 3D) is based on block copolymers, through the microphase separation of covalently connected blocks with chemical dissimilarity.[1] A fundamentally different approach is based on the Watson-Crick chemical complementarity, a programmable self-assembly method that offers a powerful tool for designing all-DNA multidimensional functional complex structures with unparalleled control over nanoscale-domain geometry.[2–5]

Although the DNA base specificity is the greatest advantage in DNA-based self-assembly, it can also be the Achilles heel. Increasing the design complexity of the target structure requires a large number of DNA strands with unique sequences, which not only raises serious scalability issues but also unavoidably introduces errors in self-assembly, leading to short-range ordered structures. A synergy of these two chemically and conceptually distinct self-assembly pathways can offer alluring opportunities to generate tailored macroscopic DNA-based reconfigurable soft materials that could circumvent the above mentioned limitations, while retaining their sequence addressability. So far, this idea remains limited to the construction of micelles, vesicles, nanotubes and ordered nanofibers from DNA-polymer.[6–13] To realize the full potential of the combination of block copolymer self-assembly and programmed DNA self-assembly in the field of structural DNA nanotechnology, the formation of highly ordered multidimensional arrangement of DNA blocks is highly desirable.

Here, we demonstrate a robust pathway on achieving the above goal, based on the fabrication of DNA-based anisotropic soft-patchy particles, comprising a charged rigid DNA rod and a neutral thermo-sensitive flexible polymeric segment (Poly(N-isopropylacrylamide), pNIPAm) that are covalently linked. Typical examples are presented in Figure 1, where the pNIPAm polymer can be either linked to the ends of a stiff linear DNA fragment (see Figure 1a) or to programmed sites along the DNA fragment (Figure 1b), or to the ends of a star-shaped DNA construct with stiff arms (Figure 1c). The key ingredient of the proposed self-assembly strategy, based on the block copolymer paradigm, is the microphase separation mechanism driven by the immiscibility between the rod-like DNA-block and the coil-like pNIPAm-block. A similar approach was employed for the self-assembly of anisotropic inorganic particles in linear and circular polymer-like structures by functionalizing hydrophilic gold nanorods at both ends with hydrophobic homopolymer.[14]

Broadly speaking, the proposed system has many features in common with the conventional block copolymers, so that the equilibrium self-assembled morphologies will be governed by similar fundamental physical principles: the compromise between minimizing unfavorable contacts between the incompatible blocks and maximizing the system's configurational entropy. In our DNA-polymer hybrids, however, the combination of multi-blocks in one system having tunable enthalpic, entropic and charge disparities have profound consequences concerning their associated self-assembly behavior. In comparison to traditional uncharged flexible block copolymers, additional entropic contributions will be present in the system's free energy, leading to rich phase transitions pathways and intriguing complex phases, as demonstrated in the present work. These contributions are related to the anisotropic shape of the DNA-block that can result in the formation of anisotropic liquid crystal phases,[15–18] and to the entropy of counterions owing to the charged character of the DNA-block.[19,20] Furthermore, from the enthalpic point of view, the temperature-dependent solvophobicity of the pNIPAm-block allows the external steering of the degree of amphiphilicity of our system, thus offering a way to fine control the segregation strength between the blocks forming the proposed DNA-based block copolymers. Our findings on self-assembly of the reported DNA-polymer constructs constitute an experimental realization of the pioneering concept for nanoparticle self-assembly based on the "precise positioning of tethers on the surfaces of nanoparticles of arbitrary geometry and composition", as suggested by simulation study more than a decade ago.[21]

Results and discussion

Synthesis of DNA-polymer hybrids. Our synthetic scheme involves sequence-specific post-decoration of stiff double-stranded DNA (dsDNA) fragments with pNIPAm polymer chains employing copper-free click chemistry[22] (more details are given in the Method section and Supporting Information, Sections 1.1-1.3). pNIPAm is a temperature-responsive polymer with lower critical solution temperature behaviour at T $\sim$ 33°C in salt-free aqueous solutions. The length of the dsDNA fragment is well below its persistence length ($\sim$ 50 nm) and therefore the DNA fragments can be considered as stiff rods. The term "soft-patchy", used to describe the proposed anisotropic DNA-based particles, refers to the polymeric nature of the patchy units (pNIPAm) in which shape and position fluctuations are allowed. These features are absent in the conventional "hard-patchy"particles,[23,24] and, as we shall demonstrate, they have a profound effect on the dominant self-assembly pathways. Non-denaturing gel electrophoresis was employed to confirm the successful assembly of the DNA-polymer architectures which are schematically depicted in Figure 1a-c. The electrophoresis experiments presented in Figure 1d-e were performed on the crude reaction mixtures with the optimal ratio of reacting compounds. The desired DNA structures migrate as a single sharp band, suggesting that DNA-polymer conjugates were properly formed (see Supporting Information, Section 1.4 and Figures S1-S3 for more details). In terms of block copolymer architecture, the three proposed DNA-based soft-patchy particles resemble a linear-shaped coil-rod-coil triblock (L-CRC), Π-shaped rod-coil triblock (Π-RC) and star-shaped diblock with rod-coil arms (S-RC).

We shall demonstrate the proposed conceptual strategy for encoding information into self-assembling DNA building blocks by presenting the temperature dependence of the self-assembly behavior of the above-mentioned DNA-based anisotropic soft-patchy particles in aqueous solutions, at selected DNA concentrations, employing small-angle X-ray scattering (SAXS) experiments (see Methods for details) and optical depolarized light observations of the samples.

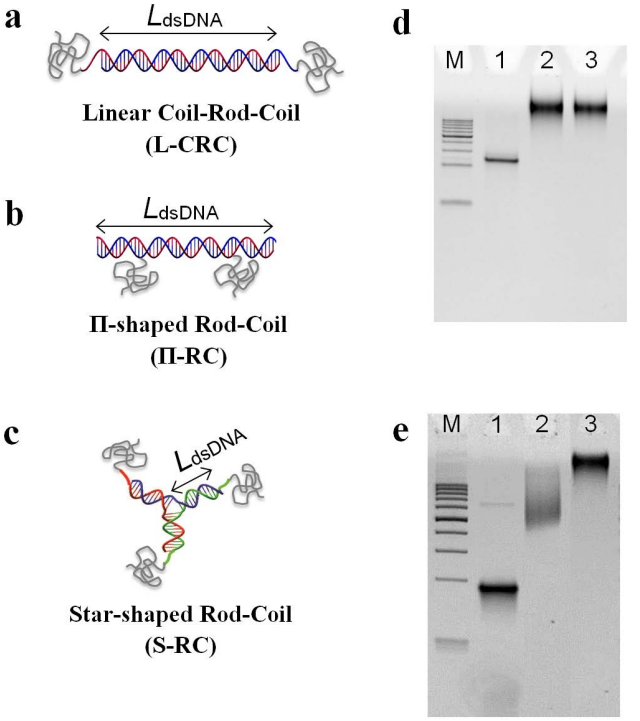

Figure 1: **Synthesis and characterization of DNA-based anisotropic soft-patchy particles.** Schematic representation of the DNA-polymer particles used for the exploration of the self-assembly behavior of patchy rod-shaped molecules. **a,** Linear-shaped coil-rod-coil triblock (L-CRC). **b,** Π-shaped rod-coil triblock (Π-RC). **c,** Star-shaped diblock with rod-coil arms (S-RC). The cartoons (**a-c**) approximately capture the relative length scales in our DNA-polymer hybrids **d-e,** Non-denaturing polyarcylamide gel electrophoresis (PAGE) analysis. (**d**) 15% PAGE. Lane M contains 20 base-pair (bp) DNA marker. Lanes 1-3 contain dsDNA fragment, coil-rod-coil (L-CRC) and Π-shaped rod-coil (Π-RC) respectively, with a length of $L_{\text{dsDNA}} = 48\,\text{bp} \sim 16\,\text{nm}$ (using 0.33 nm per base-pair) and pNIPAm with molecular weight of 20KDa. (**e**) 10% PAGE. Lanes M-1 contain 50bp DNA marker and three-arm dsDNA junction (Y-DNA) respectively, with arm length of $L_{\text{dsDNA}} = 13\,\text{bp} \sim 4.4\,\text{nm}$. Lanes 2-3 contain the Y-DNA of lane 1 functionalized with 1.7 KDa and 20 KDa pNIPAm (S-RC), respectively. For the 20KDa pNIPAm, the hydrodynamic radius is about 3.5 nm in the swollen state.

Phase behavior of the L-CRC for concentrations well below the liquid crystal ordering of DNA-block. One-dimensional SAXS (1D-SAXS) profiles, at 4^{o}C for the bare DNA-block with a fixed length $L_{\mathrm{dsDNA}} = 48\,\mathrm{bp} \sim 16\,\mathrm{nm}$, are shown in the top panel of Figure 2a for various concentrations. These profiles are obtained by azimuthally-averaging scattering intensity of a two-dimensional SAXS (2D-SAXS) scattering pattern, an example of which is shown in Figure 2b. With increasing DNA concentration, the DNA-block is found to exhibit the liquid crystal behavior typical for DNA.[25] Two-phase coexistence develops at the transition from the isotropic to chiral nematic transition, as demonstrated in the images in Figure 2a (inset of top panel) taken through cross polarizers. The isotropic to biphasic transition concentration is found to be around $170\,\mathrm{mg/ml}$. For concentrations well above the isotropic-to-chiral nematic transition, the 1D-SAXS profile (Figure 2a, top panel, black curve) reveals a single intense and narrow Bragg reflection. This correlation peak originates from a strong positional order between neighboring, parallel DNA helices and is associated with the formation of a hexagonal-columnar DNA mesophase.[26,27]

Incorporation of a pNIPAm-block at the ends of the DNA-block, which yields the formation of the L-CRC system presented in Figure 1a, drastically affects the associated phase behaviour. While DNA concentration is below the critical value required for the liquid crystal (LC) phase formation ($\mathrm{c_{LC}} \sim 195\,\mathrm{mg/ml}$) and the temperature is far below the lower critical solution temperature of the pNIPAm-block, the image of the sample taken through cross polarizers reveals the formation of a strongly birefringent phase (similar to Figure 2f). A further striking difference is the shape of the SAXS profile for the L-CRC system and the unmodified DNA-block at the same DNA concentration and temperature, as can be seen from the comparison of the scattering profiles presented in the top (brown curve) and bottom panel of Figure 2a. For the L-CRC, a clear shift of the value of $\mathrm{q_{DNA}}$ peak to higher q, and a significant narrowing of its width are observed. This suggests strong positional correlations between the DNA-blocks. In addition, the L-CRC system shows a sharp principal scattering peak at a wavevector $\mathrm{q^*}$ and several higher-order reflections, with wavevector ratios $\mathrm{q/q^*}$ of 1:2:3:4. Such higher-order reflections are indicative of a lamellar (Lam) structure. The position of the primary peak $\mathrm{q^*}$ corresponds to a layered structure with a spacing between adjacent layers of $\mathrm{d_{Lam}} = 2\pi/\mathrm{q^*} = 28\,\mathrm{nm}$. Information concerning the arrangement of the DNA-block in the layers can be obtained by observing 2D-SAXS patterns of a shear-aligned sample,[25] an example of which is given in Figure 2b. The peaks originating from correlations between the lamellar planes (arcs close to the beam stop) are oriented exactly perpendicularly to the peaks originating from correlations in DNA diameter (the outer broad arc, which corresponds to the $\mathrm{q_{DNA}}$ peak in the 1D-SAXS profile). This clearly implies that the DNA-blocks of the L-CRC system within the layers are oriented parallel to the layer's normal.

Further analysis of the 1D-SAXS profile of Figure 2a (bottom panel), based on a combined model able to describe in detail the lamellar structure as well as the DNA-block local packing inside the lamellar domains, revealed that the average coherent domain size, $\mathrm{D_{Lam}}$, in the direction perpendicular to the lamellar layers is close to 1.2μm (details on the fitting procedure of the 1-D SAXS profile and the model employed are given in Supporting Information, Sections 2.1-2.2 and Figure S4). In addition, the extracted value for the in-layer positional correlation length λ_{D}, as calculated from the width of the narrowed $\mathrm{q_{DNA}}$ peak, reveals the formation of well-ordered domains of dimension $\lambda_{\mathrm{D}} = 314nm$; this suggests that about 100 DNA helices pack in coherent manner within the DNA layers. A schematic of the above packing scenario for the L-CRC system is presented in Figure 2c, consisting of uncorrelated layers in which the molecules are positioned in a hexagonally close packed array (smectic-B type of liquid crystal phase).

By increasing the temperature, an unexpectedly rich phase transition pathway from lamellar to various cubic network phases is observed. The SAXS signature of this multiple order-to-order morphological transition is shown in Figure 2d for the L-CRC at DNA concentration of $119.3\,\mathrm{mg/ml}$. Up to 23^{o}C, a temperature quite below the lower critical solution temperature of the pNIPAm-block, the L-CRC exhibits ordered lamellar structure charac-

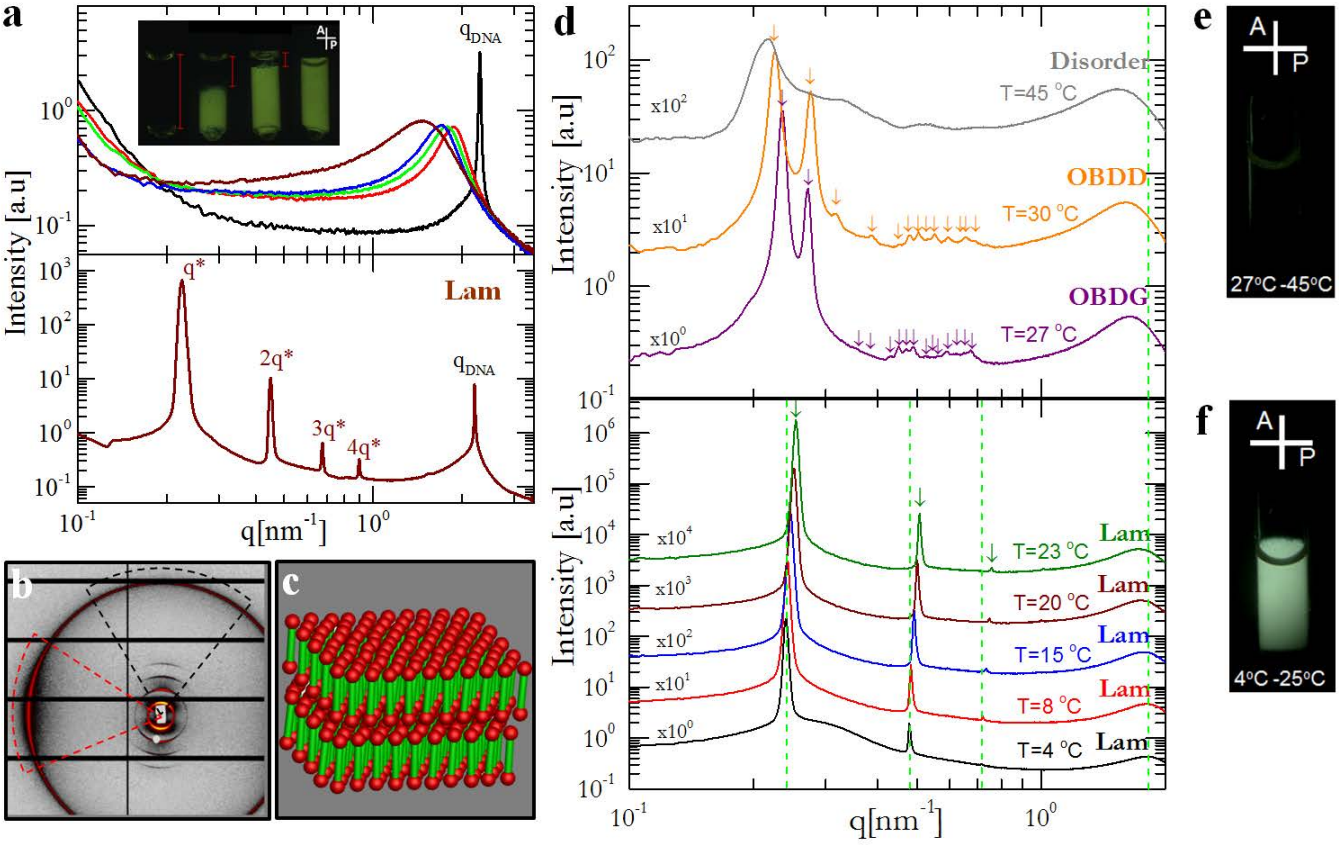

Figure 2: **Self-assembly of polymer-tethered DNA nanorods**. **a,** Top panel: SAXS profiles for the bare DNA-block, with total concentrations are 278.0 (black), 238.0 (red), 216.5 (green), 183.5 (blue) and 171.0 (brown) mg/ml. The inset shows pictures of selected samples between cross-polarizers in one-phase and two-phase coexistence (total concentrations from left to right: 171.0, 183.5, 190.0, and 206.0 mg/ml).The red bars indicate the height of the isotropic region. The SAXS profile for the duplex at 183.5 mg/ml is taken from the liquid crystal region of the second capillary from the left in the inset photograph. Bottom panel: SAXS profile for the coil-rod-coil (L-CRC) at a concentration of 163.0 mg/ml. The SAXS profiles were taken at 4°C. **b,** 2D-SAXS pattern for a shear-aligned sample of the coil-rod-coil (L-CRC) at 163.0 mg/ml. **c,** Schematic of the proposed arrangement of the coil-rod-coil (L-CRC) molecules in the lamellar. The DNA and polymer are illustrated as cylinder and ball, respectively. **d,** Temperature-dependent SAXS profiles of the coil-rod-coil (L-CRC) at 119.3 mg/ml. The arrows indicate the relative positions for the first possible reflections for the stated morphologies. Profiles are shifted along the intensity axis for clarity. The intensity shift factors are presented on the left side of the profiles. The most right green dashed line is guide for the temperature dependence of the q_{DNA} peak. The remaining green vertical lines are added to indicate the temperature dependence of the location of the q* peak, as well as the higher order reflections related with the lamellar morphology. **e-f,** Depolarized images of the L-CRC sample with a concentration of 119.3 mg/ml at different temperatures.

terized by a macroscopically uniform birefringent pattern, as evident by the depolarized image given in Figure 2f. The considerable q_{DNA} peak broadening indicates a liquid-like positional order between the DNA-blocks inside the lamellar layers, in opposition to the sharp peak observed at the higher concentration (Figure 2a, bottom panel). Heating the sample produces a gradual shift of the reflections towards higher q values. Since the pNIPAm-block is the only block in the L-CRC system that is conformational sensitive to temperature, the decrease of the layer spacing is attributed to a shrinkage of the pNIPAm-block upon heating. The change in the lamellar spacing due to the pNIPAm conformational change is paired by an increased distance between neighboring, parallel DNA helices within the DNA-block layers with increasing temperature, as revealed by the shift of the maximum of the q_{DNA} peak to lower q values.

The effective swelling of the DNA-block layer persists up to 23^{o}C, where a slightly further temperature increase induces a markedly different phase, as can be seen from the SAXS profiles in Figure 2d. More specifically, the L-CRC undergoes a sequence of phase transitions from a lamellar (Lam, 23^{o}C) to an ordered bicontinuous double-gyroid phase (OBDG, 27^{o}C), and finally approaching, but still below the lower critical solution temperature of the pNIPAm-block, to an ordered bicontinuous double-diamond phase (OBDD, 30^{o}C) upon heating. The SAXS profiles for the bicontinuous cubic phases are shown in Figure 2d together with the expected peak positions for OBDG and OBDD morphologies with $Ia\bar{3}d$ and $Pn\bar{3}m$ space group symmetries,[28–31] respectively (purple and orange arrows in Figure 2d). The intense first two sharp peaks, the quite large number of lower intensity but clearly distinguishable high-order reflections in our SAXS profiles, and the excellent agreement between the observed peaks and the allowed reflections, offer compelling evidence regarding the morphology of the above-mentioned cubic network phases with a significant long-range order. In addition, the reported bicontinuous cubic phases are attested by the absence of optical birefringence at temperatures above 23^{o}C, as clearly illustrated in the depolarized image of Figure 2e. Ultimately, at 45^{o}C, a temperature well above the lower critical solution temperature of the pNIPAm-block, the sample disorders, resulting in the abrupt disappearance of the two principal peaks as well as the higher order peaks. It is worth mentioning that, in contrast to OBDG, the OBDD structure in conventional block copolymers melts consisting solely of flexible polymer chains has not been considered as a thermodynamically stable phase due to fact that high levels of packings frustration are encountered.[32,33] However, our SAXS results demonstrate an unexpected ease on stabilizing the OBDD phase (also see Supporting Information, Section 3.1 and Figure S7), suggesting that block rigidity (DNA-block) may play a key role in the formation of this cubic network phase. Even though the addition of solvent to block copolymers (water in our case) imparts additional degrees of freedom to control the final self-assembled morphology, we believe that the entropic penalty associated with the pNIPAm chains packing is effectively counterbalanced by the tendency of the rod-like DNA-blocks to align (liquid crystal ordering). The latter ordering mechanism is absent in convectional block copolymers consisting solely of flexible chains.

In Figure (Supporting Information, Section 3.1), a thermal scanning SAXS experiment over a small temperature increment for the L-CRC system is presented; the DNA concentration is slightly higher than that of Figure 2d. The same multiple order-to-order transitions (Lam-to-OBDG-to-OBDD) are observed by increasing the temperature. The 1D-SAXS profiles reveal that at 27^{o}C and at 30^{o}C there is a coexistence of peaks from Lam/OBDG and OBDG/OBDD, respectively. This indicates a discontinuous transition for the Lam-to-OBDG and OBDG-to-OBDD cases. However, the SAXS signature at the proximity of these order-to-order transitions does not allow a conjecture regarding the order type of these phase transitions. It is important to emphasize that the above order-to-order transitions (Lam-to-OBDG-to-OBDD) are reversible with temperature, and stable with prolonged annealing (see Supporting Information, Section 3.1 and Figure S9). In addition, the kinetics of the ordering processes is quite rapid with equilibration times after temperature changes of less than 5 min., both on cooling and heating (see Supporting Information, Section 3.1 and Figures S9-S10). Therefore, we conclude that the observed multiple order-order phase transition pathway re-

flects thermodynamically equilibrium morphologies, with well-defined transition temperatures.

Phase behavior of the L-CRC for concentrations above the liquid crystal ordering of the DNA-block. Elevation of the L-CRC concentration well above the critical value c_{LC} required for liquid crystal ordering of the DNA-block, a significant change in the topology of its phase diagram is observed by means of SAXS measurements (Figure 3). The temperature-induced phase sequence from lamellar to multiple cubic network morphologies ($c < c_{LC}$) is replaced by lamellar to hexagonally packed cylinders (HPC with P6/mm symmetry) morphology ($c > c_{LC}$), as clearly demonstrated in Figure 3a, in which SAXS profiles at selected temperatures together with the expected reflections are presented. The lamellar periodicity ($d_{Lam} = 2\pi/q^*$) and the distance between the centers of adjacent cylinders ($d_{HPC} = 4\pi/\sqrt{3}q^*$) are found to be 28.5 nm and 33.5 nm, respectively. Analysis of the 2D-SAXS patterns obtained for a shear-aligned L-CRC sample at $T = 20^oC$ and $T = 25^oC$ allows the identification of the arrangement of the DNA-block inside the proposed 1D (Lam) and 2D (HPC) long-range ordered nanostructures. The relative orientation of the arcs associated with the proposed structures to the arc corresponding to q_{DNA} peak, and analysis of the SAXS profile at $T = 25^oC$, reveal a temperature-induced transition from a Lam (Figure 3e) to HPC morphology in which the DNA-blocks are packed within the cylinders with a diameter $d_{cyl} = 20$ nm slightly larger than one DNA-block molecular length (Figures S5). The extracted value for the cylinder diameter in the HPC morphology, under the assumption of cylinders with circular cross-section, is quite intriguing since it hints at the possibility of DNA-blocks packing within the cylinders such that they induce twist about the cylinder axis, thus forming chiral nematic cylinders. On the basis of geometrical arguments using the calculated values for the cylinder diameter, the interdomain spacing, and the interaxial distance between the DNA-blocks (for more details, see the analysis of 1D-SAXS profile at $T = 25^oC$ in Figure S5 and relevant discussion in Supporting Information, Sections 2.1, 2.3), we propose the packing model of Figure 3d, in which the cylinder cross-section contains at most five L-CRC molecules.

This scenario is plausible given the chiral nature of DNA[34] and the entropy gain due to more efficient packing of the coil-like pNIPAm-blocks. It is worth mentioning that existing simulations studies on the self-assembly of polymer-tethered achiral nanorod model system predicted the formation of such a intriguing hexagonal cylinder phase consisting of chiral cylinders.[35] However, the analysis of the shear-aligned 2D-SAXS pattern does not allow a conjecture regarding the shape of cylinder's cross-section in HPC morphology and therefore we can not exclude the possibility that the DNA helices pack in parallel within a cylinder of rectangular cross-section. A computational study employing a coarse-grained model of our polymer-tethered chiral charged nanorods (L-CRC system) could provide a deeper insight into the local structure within the cylinders in terms of chiral pitch (twist periodicity) and handedness. Finally, it would be interesting to explore if the grafted-like pNIPAm chains on the cylinders surface can screen the chiral interactions, stabilizing the straight column configuration as shown in Figure 3d or to a possible racemic mixture of hexagonally ordered chiral cylinders.[35]

Phase-diagram of the L-CRC. The phase behavior of L-CRC system as a function of temperature and concentration is presented in Figure 4. The temperature-induced phase sequences for DNA concentrations well below ($c \leq 130$ mg/ml) and above ($c \geq 205$ mg/ml) the critical value c_{LC} required for liquid crystal ordering of the DNA-block are already discussed in detail in the previous sections. Approaching the c_{LC} ($c \geq 130$ mg/ml, the increase of temperature results in a transition from a lammelar phase to different unidentified complex phases (colored region in Figure 4). Their SAXS patterns based on the position of the first two intense Bragg reflections can be indexed to OBDG and OBDD structures, and in some cases, higher order reflections are consistent with the expected peak positions for these morphologies with $Ia\bar{3}d$ and $Pn\bar{3}m$ space group symmetries, respectively (Figure S8). However, depolarized images of the samples reveal an intense uniform birefringence (similar to figure 2f), hence the formation of such cubic network phases can be excluded.

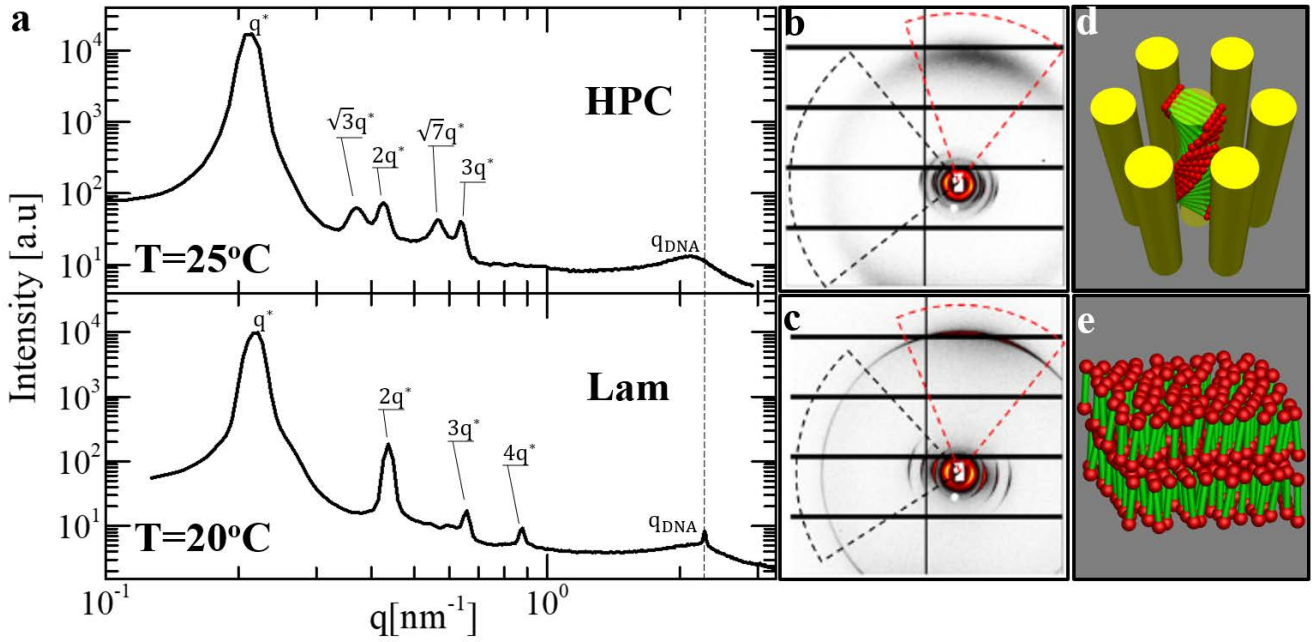

Figure 3: **Self-assembly of coil-rod-coil (L-CRC) system for $c > c_{\mathbf{LC}}$. a,** SAXS measurements of the coil-rod-coil (L-CRC) at a concentration of 210.3 mg/ml for $T = 20^oC$ (bottom panel) and $T = 25^oC$ (top panel). The 1-D scattering curves are obtained from azimuthally averaged the region (black cake-like) indicated in the corresponding 2D-SAXS patterns (**b-c**). The positions of the higher order reflections with respect to that of the first (and most intense) peak, q^*, are also depicted. The black dashed line is a guide for the temperature dependence of the q_{DNA} peak. **b-c,** The 2D-SAXS patterns for a shear-aligned sample of the coil-rod-coil (L-CRC) system at $T = 25^oC$ (**b**) and $T = 20^oC$ (**c**); the red colour corresponding to the highest intensity. The black and the red cake-like regions indicate the relative orientation of the arcs associated with the proposed structures to the arc corresponding to q_{DNA} peak. **d-e,** Possible scheme of the packing arrangement of the coil-rod-coil (L-CRC) molecules inside the lamellar (**e**) and hexagonally packed cylinders (**d**) structures. The DNA and polymer are illustrated as green cylinder and red ball, respectively.

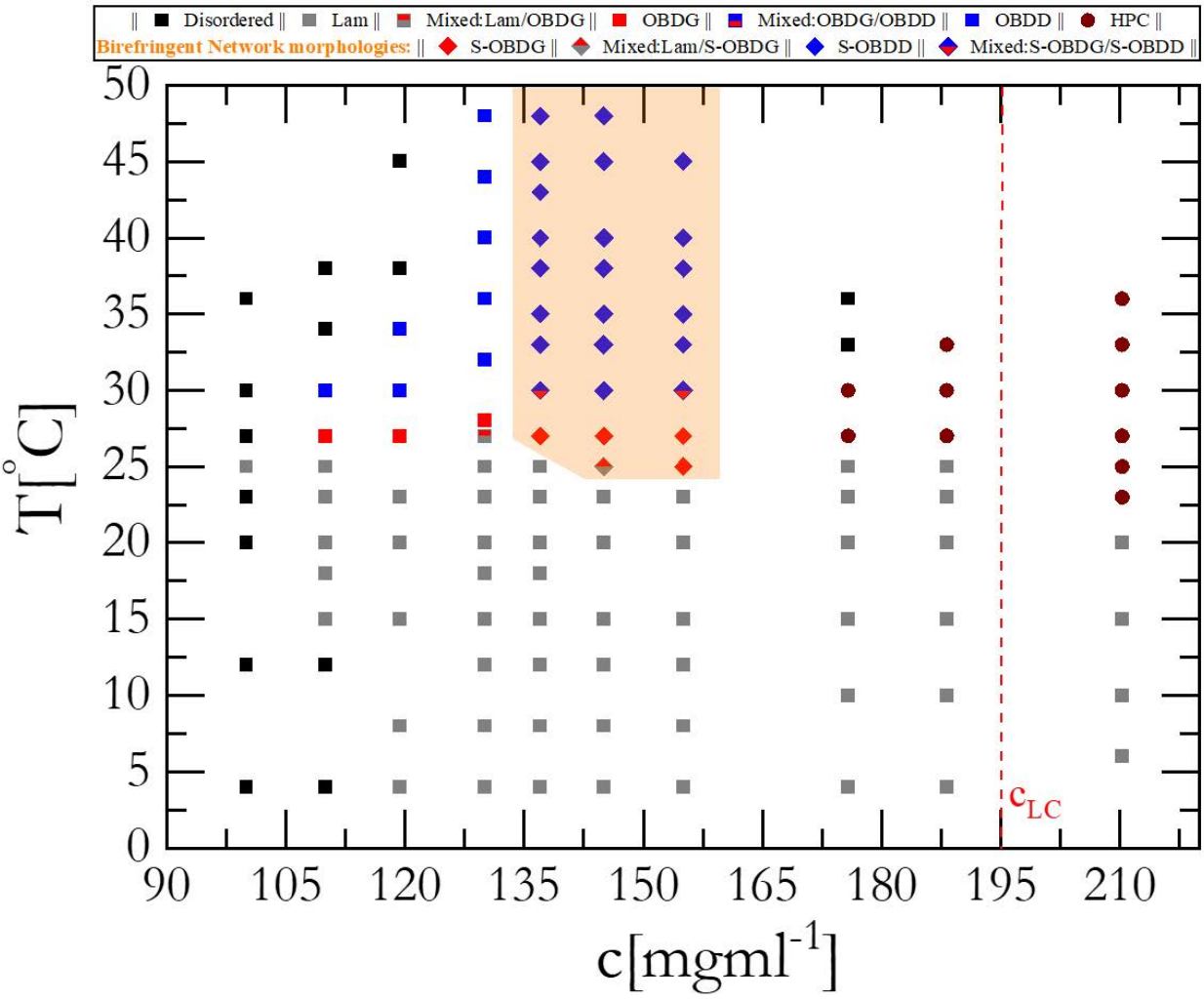

Figure 4: **Phase behavior of coil-rod-coil (L-CRC) system.** A representative phase diagram of the L-CRC system as a function of temperature (T) and DNA concentration (c). The symbols indicate the samples that were loaded into capillaries for SAXS measurements. The colored region of the diagram contains unidentified, most likely non-cubic network morphologies (S-OBDG: non-cubic lattice with double-gyroid-like morphology; S-OBDD: non-cubic lattice with double-diamond-like morphology). The red dotted line marks the critical value c_{LC} required for liquid crystal ordering of the DNA-block. The color code for the different phases is given in the top of the figure (Lam: Lamellar, OBDG: Ordered Bicontinuous Double-Gyroid, OBDD:Ordered Bicontinuous Double-Diamond, HPC: Hexagonally Packed Cylinders, S-OBDG: Stretched OBDG, S-OBDD: Stretched OBDD).

We therefore speculate that these structures more likely correspond to stretched double-gyroid (S-OBDG) and double-diamond (S-OBDD) network morphologies.

Noncubic network structures with an orthorhombic unit cell have been encountered in block polymer materials.[33] The identification of such anisotropic network structures and their assignment to a specific non-cubic lattice with a particular crystallographic space group symmetry requires 2D-SAXS patterns from nearly single crystalline grains. Our powder diffraction patterns with limited number of higher-order reflections don't allow such a unique Bragg peak indexing. Synchrotron microbeam SAXS experiments on macroscopically aligned samples could provide an unambiguous evidence about the emergence of such anisotropic double-network phases in our L-CRC system, which will be the subject of future work.

Brownian Dynamics simulations of model L-CRC system. To resolve the structure of the L-CRC system in the OBDG and OBDD phase for $c < c_{LC}$, we performed Brownian Dynamics (BD) simulations of a coarse-grained model of rod-like colloids with attractive ends[36] (Figure 5a; more details regarding the simulation are given in the Methods and Supporting Information, Section 4). Lipid-water mixtures typically exhibit a phase transition from a lamellar to a double-gyroid phase with increasing water content, where lipids are arranged in sheets, which minimize the contact between hydrocarbon tails and water.[37] The Figure S13 displays corresponding bicontinuous OBDG and OBDD phases. However, our simulations show that these structures for L-CRCs are unstable. The indication of mechanical stable phases is only obtained for L-CRC concentrations exceeding the experimental values by far, which rules out such an arrangement of L-CRC molecules. In contrast, the simulations indicate that bicontinuous cubic network structures consisting of bundles of L-CRC molecules are stable for sufficiently strong end-attraction strengths. These structures are illustrated in Figure 5b-c, which are consistent with the experimentally obtained unit cell sizes and number of molecules per cell (see Methods, Supporting Information, Section 4 and Figure S14 which demonstrates the role of end-attraction strength in the mechanical stability of cubic network phases). Interestingly, the OBDG structure comprises 2- and 3-fold coordinated nodes. Simulations reveal that a OBDG structure with only 3-fold coordinated nodes is less mechanically stable (see Figure S17). Hence, for $c < c_{LC}$, a temperature increase implies pronounced structural rearrangements from a lamellar phase of L-CRC molecules to bundles of L-CRCs linked by their ends. We speculate that the primary driving force that stabilizes bundle-like morphology at the expense of the sheet-like morphology is rooted in the rod-like character of the DNA-block. The formation of sheet-like structures by rigid L-CRC molecules is disfavored in bicontinuous phases with high curvatures, because of packing constraints and large splay. In addition, the DNA-blocks are water soluble, so that bundle formation is not disfavored by the hydrophobic effect.

The SAXS experiments presented in Figure S7, indicate that there is an overwhelming prevalence of the OBDD over the OBDG structure. In contrast, in simulations both cubic phases show comparable mechanical stability in a range of end-to-end attraction strengths around $\varepsilon/k_BT = 5$. Even though the relaxation of the energy of the OBDD-structure is slower as compared to the OBDG-structure (see Figure S16), lower energies are reached, which indicates a higher mechanical stability of OBDD, in agreement with experiments. It is important to realize, however, that the simplicity of the simulation model does not allow a quantitative comparison with the experiments (see relevant discussion in Supporting Information, Section 4). In addition, a conjecture regarding the thermodynamic stability of the proposed model L-CRC molecular arrangements for the OBDG and OBDD structures cannot be made. The aim of the performed simulations has been to access the molecular arrangement of L-CRC within the cubic network phases, the existence of which is unambiguously demonstrated by SAXS experiments.

Site-specific DNA-pNIPAm conjugates. A notable feature of the modular synthetic scheme reported here is that it allows site-specific incorporation of the pNIPAm-block on DNA with sub-nanometer precision, at the level of a single base. We demonstrate the above spatial addressability

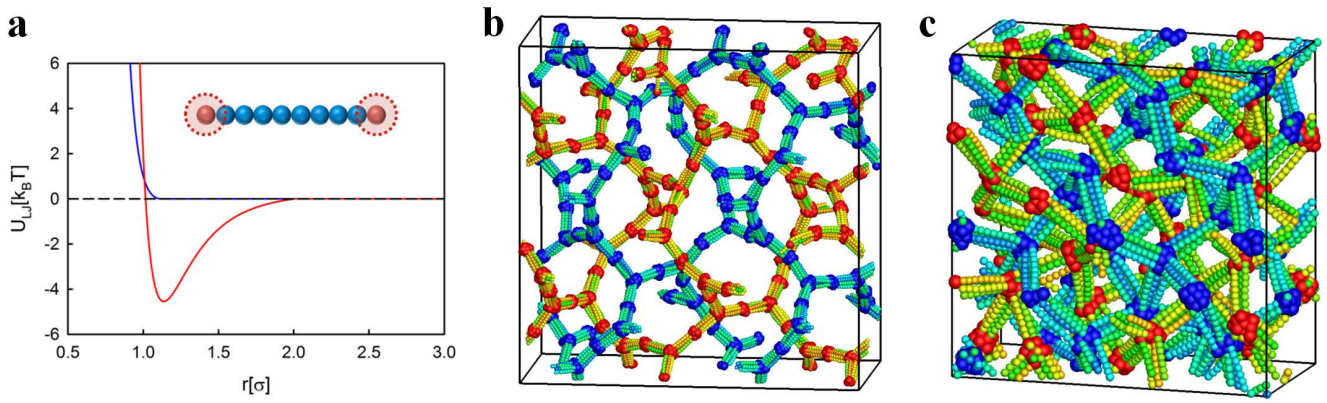

Figure 5: **Brownian dynamics simulations. a,** The schematic of the interaction model is illustrated in the inset. The coil-rod-coil (L-CRC) system is modeled as a chain of tangent beads. The DNA-block is represented by the blue beads, equally spaced along a line. The red beads, which model the pNIPAm-blocks, are attractive sites located at the free-ends of the DNA-block. The pair-interaction potentials between non-bonded beads are shown by lines. The red line corresponds to the attractive interaction potential between two end-beads. All other pair-interactions are purely repulsive and they are described by a hard-core interaction potential (blue line). **b-c,** A snapshot of the model coil-rod-coil (L-CRC) molecular configuration in equilibrium for the doube-gyroid (OBDG) structure (**b**) and for the doube-diamond (OBDD) structure (**c**). The end-attraction strength is set to $\varepsilon = 5\mathrm{k_B T}$. The two interpenetrating but non-intersecting networks formed by bundles of particles, with a mixture of 3-fold and 2-fold connectivity of each node for the doube-gyroid (OBDG) (**b**) and a 4-fold connectivity of each node for the doube-diamond (OBDD) (**c**), are generated by joining nodes in the network by a series of straight segments consisting of bundles of particles. Each bundle contains 7 DNA-blocks for the doube-gyroid (OBDG) structure and 4 DNA-blocks for the doube-diamond (OBDD) structure, which results 336 and 128 coil-rod-coil (L-CRC) molecules per unit cell, respectively. The pNIPAm-blocks are located at the nodes for both network phases.

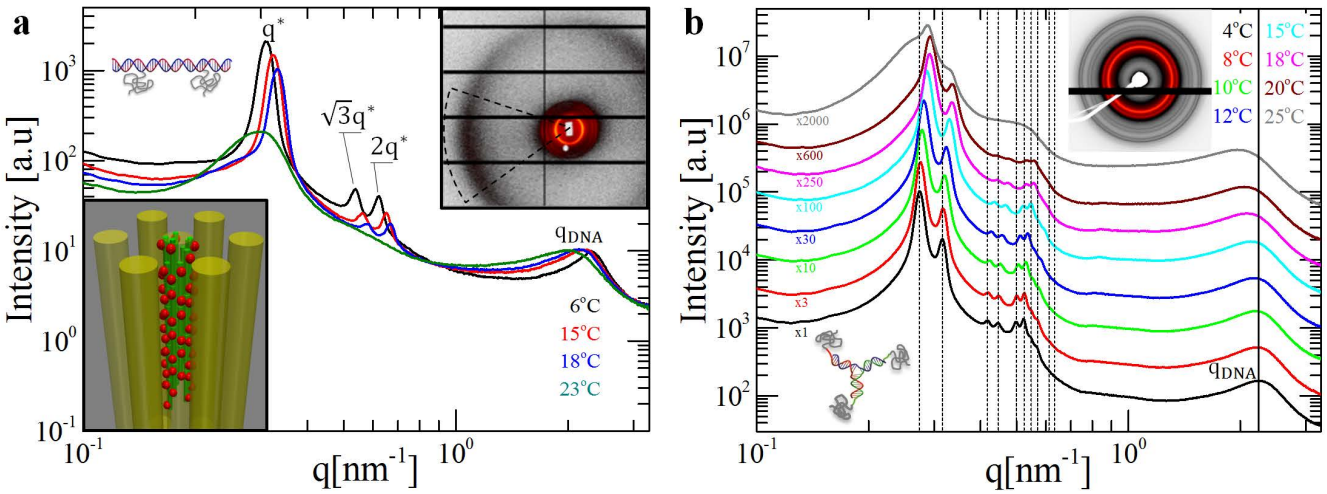

Figure 6: **Sequence-selective covalent attachment of polymeric patches on DNA**. **a,** Temperature-dependent SAXS profiles of the Π-shaped rod-coil (Π-RC) (top-left inset) at a concentration of 194.7 mg/ml (black: T = 6°C, red: T = 15°C, blue: T = 18°C and green: T = 23°C). The positions of the higher order reflections with respect to that of the first (and most intense) peak, q*, are also indicated. Top-right inset: The 2D-SAXS pattern at T = 4°C. The black cake-like region indicate the relative orientation of the arcs associated with the proposed morphology to the arc corresponding to q_{DNA} peak. Bottom-left inset: Schematic model of molecular self-organization within the hexagonally packed cylinders. The DNA and polymer in the Π-shaped rod-coil (Π-RC) systems are illustrated as green cylinder and red ball, respectively. **b,** Temperature-dependent azimuthally integrated SAXS patterns of the star-shaped rod-coil (S-RC) system (bottom-left inset) at a concentration of 213 mg/ml. Top inset: The 2D-SAXS pattern at T = 4°C. The vertical dashed lines correspond to the expected peaks for the $Ia\bar{3}d$ (consistent with a doube-gyroid (OBDG) moprhology) crystallographic space group symmetry. The doube-gyroid (OBDG lattice parameter (unit cell size, α_{DG}) equals to 56.3 nm at 4°C. Heating of the sample produces a gradual decrease of the α_{DG} by approximately 6.3% from 4°C to 18°C; and ultimately at 23°C the sample disorders. The vertical solid line is a guide for the temperature dependence of the q_{DNA} peak. Profiles are shifted vertically for clarity. The intensity shift factors are presented on the left side of the profiles.

of DNA by covalently attaching a pNIPAm-block 10 bp away from the blunt-ends of the DNA-block (more details are given in the Supporting Information, Section 1.1). The corresponding molecular Π-RC structure is presented in Figure 1b. This slight change in the position of the polymeric patches (pNIPAm-block) compared to the L-CRC system drastically affects the resulting self-assembly, as evident by the SAXS measurements on the Π-RC system (Figure 6a) at similar temperatures and concentrations as for the above discussed L-CRC system. The SAXS profiles in Figure 6a, at temperatures below T = 23°C, display three reflections located at q/q^* ratios of $1{:}\sqrt{3}{:}2$, characteristic of a 2D hexagonal-packed cylinders structure. From the observed first-order reflection, the lattice parameter d_{HPC} can be estimated to be 23.3 nm at T = 6°C. The position of the low-q peaks (associated with the HPC morphology) and the q_{DNA} peak demonstrate the same temperature dependence as for the lamellar phase in the L-CRC system, presented in the bottom panel of Figure 2d. Heating the sample produces a gradual decrease of the d_{HPC} (from 23.3 nm at T = 6°C to 21.8 nm at 18^oC) and ultimately at T = 23°C the samples disorders; the higher-order peaks disappear and the principal peak becomes broader with an abrupt decrease in its intensity.

The packing of Π-RC molecules inside the HPC morphology can be determined by observing 2D-SAXS pattern of a shear-aligned sample, an example of which is given in the right inset of Figure 6a. The innermost series of sharp diffraction peaks associated with the HPC morphology (arcs close to the beam stop) are in perfect alignment with the q_{DNA} peak originating from correlations in the DNA-block diameter (outer broad arc). This implies that, oppositely to the L-CRC, the DNA-blocks of the Π-RC system are oriented along the cylinder axis. Further evidence for this molecular arrangement is provided from the analysis of the 1D-SAXS profile at T = 6°C, which reveals the formation of hexagonally packed cylinders morphology with cylinder diameter $d_{cyl} = 12.4$ nm; a value significantly lower than one DNA-block molecular length and therefore a packing scenario based on the arrangement of the DNA-blocks within the cylinders similar to Figure 3d is implausible. In addition, the thickness of the pNIPAm-block domain ($d_{pNIPAm\text{-}block} = d_{HPC} - d_{cyl}$) is found to be quite close to the value for L-CRC case in Figure 3d (see Figure S6 and Supporting Information, Sections 2.1, 2.3 for more details).

On the basis of the above results, in conjunction with the requirement of releasing the packing frustration related to conformational entropy of the flexible pNIPAm-blocks, a possible schematic representation for the molecular organization of the Π-RC molecules into the hexagonal columnar liquid crystal phase can be constructed, as depicted in the inset of Figure 6a. In the illustration, the Π-RC molecules comprised of blunt-ended DNA helices (DNA-block, Figure 1b), are cylindrically confined according to a two-dimensional columnar nematic fashion, resulting in a liquid crystal morphology which resembles a hexagonally packed cylindrical polymer brushes. This scenario is attributed to the attractive interaction between the terminal ends of the DNA-blocks,[38,39] which induces the formation of linear aggregates with long-range orientational but short-range positional order.

Given its versatile and robust character, the synthetic scheme reported here can easily be applied to DNA nanostructures with multi-dimensional topology. As a proof of principle, we expand our method to a relative flexible DNA branched junction structure; a three-arm DNA (Y-DNA) junction with each arm length equal to 13 base pairs. Covalent attachment of a pNIPAm-block on the free ends of the Y-DNA results in the formation of the S-RC system depicted in Figure 1c. The scattering intensity profile obtained from SAXS measurement on a concentrated aqueous solution of the S-RC system at 4°C is given in Figure 6b. A series of eight diffraction peaks, along with the absence of birefringence, strongly suggest the formation of a OBDG phase.[32] Similar to the case of the Π-RC system, heating of the sample produces a gradual decrease of the OBDG lattice parameter(see also Figure S12 and discussion in Supporting Information, Section 3.2 for the temperature-dependent SAXS profiles of S-RC with significantly smaller molecular weight of the pNIPAm-block). In overall, the staggering ease of formation of cubic network structures suggests that the reported DNA-based soft-patchy constructs, in terms of self-assembled morphologies, share striking similarities with microphase

separated surfactant-water[37,40] and block copolymer solutions.[41]

Conclusions

Programmable self-assembly is a powerful bottom-up strategy for directing the order of topologically complex morphologies emerging from tunable interactions between the molecular building blocks. Rational design of these building blocks is the key for fabrication of targeted self-assembled structures.[42] Among the available building materials in this emerging field, DNA[43,44] and patchy colloids[23,24,45] are considered prominent candidates for the realization of programmed self-assembly pathways using molecular recognition and anisotropic interactions.

Here, we demonstrate and explore the physics of a hierarchical self-assembly concept based on the site-specific decoration of the surface of a minimalist all-DNA anisotropic scaffold (rods with linear and star-shaped architecture) with polymeric patches (pNIPAm-block) having temperature-controlled interaction strength. Our approach allows to encode high levels of information into self-assembly building blocks (DNA-polymer) in the format of directionality in their interactions, resulting to an intriguing blending of ordering mechanisms originated from three distinct self-assembly platforms; block copolymers, liquid crystals and patchy particles. These short-ranged interactions were controlled by combining shape anisotropy of the building blocks (liquid crystal ordering) and chemical patterning of their surfaces (patchiness). One of the key attributes of our approach is the experimental realization of an unconventional type of patches, so called "soft-patches". The polymeric nature of these patches (pNIPAm) endows our building blocks with the microphase separation mechanism of the pNIPAm tether and the DNA rod (block copolymer ordering), imposing packing entropy constraints. Also, the segregation strength between the pNIPAm and the DNA blocks in our DNA-polymer hybrids can be temperature-controlled due to the pNIPAm's low critical solution temperature behavior, allowing access from the weak- to the strong-segregation regime. Finally, each monomer (base-pair) in the DNA scaffolds of our DNA-pNIPAm hybrids is fully addressable. This characteristic, which is absent in conventional synthetic polymers, allowed the programmable positioning of pNIPAm polymer patches on the DNA surface (Π-RC molecules). We would like to emphasize that the size of the pNIPAm chains are significant smaller than the length of the DNA rod-like block, and, therefore the former can be considered as well-defined surface patches.

At this point, it should be stressed that our self-assembly approach is fundamentally different from the DNA-based "patchy particle" self-assembly platform which is based on the programmable DNA sticky-ends interactions.[46–49] In our DNA-polymer hybrids, the use of DNA confers our building blocks with full addressability and engineered shape anisotropy. On the other hand, the arrangement of polymers at user-prescribed positions on the DNA surface offers instructions for the morphological control of the final assembled structure. The process can be readily controlled by altering the temperature and the block fraction. By using a short double-stranded DNA fragment, the simplest DNA building block (motif) for constructing DNA-polymer hybrids, we have reported high levels of self-assembled structural complexity. It is apparent that the extension of our self-assembly strategy to DNA building blocks with complex architecture is a route to design and fabricate even more intricate structures. Fortunately, advances in the field of structural DNA nanotechnology[44] have already unleashed seemingly unlimited number of rigid multidimensional all-DNA motifs with any desirable shape anisotropy (rods, multi-helix bundles, boards, discs, cubes, pyramids, supramolecular polyhedral *etc.*) and size (from nanometer up to micron using the origami technology) that could serve as an unlimited palette of rigid DNA scaffolds for our self-assembly approach. However, an a priori design of the all-DNA geometry for the realization of programmable colloidal self-assembled nanostructures is a challenge. To encode such "assembly information" into the proposed DNA-polymer building blocks requires the knowledge of how shape-based excluded volume interactions contributes entropically to self-assembly. Recent Monte Carlo simulations[50,51] have demonstrated that these directional entropic

forces can be fine controlled through the engineering of particle shape anisotropy to direct the formation of a particular crystal structure. The use of this computational approach to the proposed DNA-polymer building blocks could provide an important step toward the realization of a powerful programmable self-assembly strategy.

It is imperative to note that, nowadays, with the rapid pace of development in the field of inorganic particle synthesis, the fabrication of nanoparticles with arbitrary geometry is feasible. However, it is extremely challenging to realize their controlled surface patterning and/or functionalization.[14,49] The use of all-DNA nanostructures as scaffolds could overcome this important limitation since synthetic chemistry (as demonstrated in the Method section and Supporting Information, Section 1) enables the modification of the nucleobases in the interior and the exterior of these structures, and therefore, allowing the programmable positioning of different elements, such as polymers and inorganic nanoparticles.

The proposed self-assembly platform with a programmable character could enrich substantially the available toolbox for structural DNA nanotechnology.[52] Specifically, the ease of formation of periodic and inter-connected network structures (cubic network phases), together with their potential post-assembly stabilization by chemically photo-crosslinking the pNIPAm-based nodes[53,54] and the spatial addressability of DNA, could be of interest to diverse applications. The most prominent examples include applications in areas such as photonic crystals[55–58] and/or plasmonic materials[59] based on the use of our DNA-based cubic networks as scaffolds to position nanoparticles into a diamond cubic lattice,[58] batteries/ion transport[19] and bio-inspired materials with engineered pore structures for synthetic membranes.[60]

Methods

Synthesis of L-CRC, Π-RC and S-RC. Custom and azide (N3)-modified oligonucleotides were purchased from Biomers and purified by HPLC. The DNA concentration was determined by measuring the absorbance at 260 nm with a microvolume spectrometer (NanoDrop 2000). Each DNA construct was assembled by mixing a stoichiometric quantity of the strands involved in the L-CRC, Π-RC and S-RC in 1xTE/Na buffer (10mM Tris, pH 7.5, 0.1mM EDTA, 150mM NaCl). The final concentration was 10μM for each strand. The oligo mixtures were cooled slowly from 90^{o}C to room temperature in 10 Liter water placed in a styrofoam box over 48 hours to facilitate strand hybridization. 10% non-denaturing polyacrylamide gel (Biorad) run in 1xTBE (90mM Tris-Borate, 2mM EDTA, pH=8.3) buffer was used to confirm the assembly of linear and three-arm DNA duplexes. More details regarding the DNA sequences used for the assembly of L-CRC, Π-RC and S-RC systems are given in Supporting Information, Section 1.1. A strain-promoted alkyne-azide cycloaddition (SPAAC, copper-free click chemistry) reaction was employed for the fabrication of DNA-polymer constructs (see for details, Supporting Information, Sections 1.2-1.3). The electrophoresis experiments presented in Figure 1 were performed on the crude reaction mixtures with the optimal ratio of reacting compounds. The desired DNA structures migrate as a single sharp band, suggesting that DNA-polymer conjugates were properly formed (see for details, Supporting Information Sections 1.4). The molecular weight of the pNIPAm-block is equal to 20 KDa, unless otherwise stated.

Sample preparation. The samples were step-like diluted with buffer solution (10mM Tris, pH 8.0, 150mM NaCl) from highly concentrated solutions. The highest DNA concentration was prepared using a SpeedVac concentrator (Eppendorf). In every dilution step the DNA solution was thoroughly homogenized (up to 3 days for the more viscous samples) ensuring the absence of spatial concentrations gradients before loading into capillaries for SAXS experiments.

Small-angle X-ray scattering. Synchrotron-based SAXS (S-SAXS) measurements were carried out at the Dutch-Belgian Beamline (DUBBLE) station BM26B[61] of the European Synchrotron Radiation Facility (ESRF) in Grenoble (France). A Linkam temperature-controlled stage (HFSX350-CAP) equipped with a LNP cooling system is employed. The precise control of liquid

nitrogen flow enables this stage to be controlled at linear cooling rates as fast as $100^{o}C/min$ or as slow as $0.01^{o}C/min$. The in-house laboratory SAXS (L-SAXS) measurements were carried out at the high brilliance Galium Anode Low Angle X-ray Instrument (GALAXI) of the Jülich Center for Neutron Science (JCNS, Germany).[62] A Dectris-Pilatus 1M detector with resolution of 981x1043 pixels and a pixel size of 172x172 μm^2 was employed to record the 2D SAXS scattering patterns from L-SAXS (Jülich) and S-SAXS (DUBBLE). The 2D SAXS patterns were integrated using FIT2D software. Bragg peaks indexing in 1D SAXS profiles was performed using the Scatter computer program. 1D SAXS profiles fitting was done using in-house written Matlab code (more details on the fitting procedure are given in Supporting Information, Section 2). DNA-based solutions were loaded into 2 mm thickness borosilicate X-ray capillaries (Hilgenberg). The capillaries were sealed and stored at 4°C for at least 1 month before used for X-ray experiments. Long term stability and reproducibility was confirmed by repeating SAXS measurements on selected samples almost one year later (S-RC system, Figure S11).

Brownian Dynamics simulations. The cubic structures were investigated by means of Brownian Dynamics simulations. The network phases were constructed such as to be compatible with molecular dimensions of the L-CRC system, concentrations and experimentally determined unit-cell sizes. The L-CRC molecules are described by rod-shaped particles with attractive ends. They are composed of N_m beads connected *via* harmonic springs with a bond potential

$$U_b = \frac{\kappa}{2} \sum_{i=1}^{N_m-1} \left(|\boldsymbol{r}_{i+1} - \boldsymbol{r}_i| - l\right)^2 \qquad (1)$$

Here, κ is the spring constant and l is the bond length. The particle rigidity is controlled by the bending potential where κ_B is the bending stiffness.

$$U_B = \frac{\kappa_B}{2} \sum_{i=2}^{N_m-1} \left(\boldsymbol{r}_{i+1} - 2\boldsymbol{r}_i + \boldsymbol{r}_{i-1}\right)^2 \qquad (2)$$

The shifted and truncated Lennard-Jones (LJ) potential

$$U_{LJ} = \begin{cases} 4\varepsilon \left[\left(\frac{\sigma}{r}\right)^{12} - \left(\frac{\sigma}{r}\right)^{6} + A \right] & r < r_c \\ 0 & r \geq r_c \end{cases} \qquad (3)$$

is used to account for non-bonded interactions, where σ is the diameter of a bead and ε the interaction energy. Good solvent conditions are assumed for the DNA-part of the L-CRCs, with the excluded-volume parameters $r_c = 2^{1/6}\sigma$, $\epsilon = k_B T$, and $A = 1/4$. For the attractive ends, we set $r_c = 2.5\sigma$, *i.e.*, the end-beads are larger than the internal beads, and $A = 2.5^{-6} - 2.5^{-12}$. The end-attraction strength ε is varied between $2.0 k_B T$ and $6.0 k_B T$. Furthermore, we set $N_m = 10$, $\sigma = l$, $\kappa = 2000 k_B T/l^2$ and $\kappa_B = 500 k_B T/l^2$.

The particles are initially arranged according to the structure of OBDG and OBDD cubic network phases. Configurations of the model L-CRC molecules, and peak positions in the structure factor are recorded after the potential energy reaches a steady value (see Figures S15, S16).

Acknowledgments

This work has been supported by the Deutsche Forschungsgemeinschaft (DFG) under the grant numbers STI 664/4-1 and JO 370/5-1. NWO is acknowledged for providing beamtime at the ESRF. G.P. and E.S. thank the BM26 staff, in particular Daniel Hermida-Merino, for their technical support during the beamtime.

Supporting Information Available

The Supporting Information is available free of charge at [URL will be inserted by publisher].

Supplemental material for synthesis and characterization of DNA-polymer hybrids, experimental and simulation details and SAXS data fitting procedures.

Author contributions

E.S. conceived the study and designed research; S.N., J.Z. and E.S. performed the DNA-polymer synthesis; N.J. and U.J. performed the polymer functionalization and characterization; S.N., J.Z. and E.S. performed the experiments; G.P. operated the DUBBLE S-SAXS beamline; E.K. and U.R. operated the Jülich L-SAXS beamline; S.N., J.Z., G.P. and E.S. analyzed the experimental data; G.P. performed the fittings in the 1D-SAXS profiles; G.G., R.G.W. and J.S.M. conceived the theoretical studies and analyzed the simulation results, J.S.M. performed the simulations; E.S. and J.K.G.D. wrote the paper with contributions from all authors.

References

(1) Bates, F. S.; Fredrickson, G. H. Block Copolymers-Designer Soft Materials. *Phys. Today* **1999**, *52*, 32–38.

(2) Seeman, N. C. DNA in a Material World. *Nature* **2003**, *421*, 427–431.

(3) Aldaye, F. A.; Palmer, A. L.; Sleiman, H. F. Assembling Materials with DNA as the Guide. *Science* **2008**, *321*, 1795–1799.

(4) Seeman, N. C. Nanomaterials Based on DNA. *Annu. Rev. Biochem.* **2010**, *79*, 65–87.

(5) Rothemund, P. W. K. Folding DNA to Create Nanoscale Shapes and Patterns. *Nature* **2006**, *440*, 297–302.

(6) Kwak, M.; Herrmann, A. Nucleic Acid/Organic Polymer Hybrid Materials: Synthesis, Superstructures, and Applications. *Angew. Chem. Int. Edit.* **2010**, *49*, 8574–8587.

(7) Li, Z.; Zhang, Y.; Fullhart, P.; Mirkin, C. A. Reversible and Chemically Programmable Micelle Assembly with DNA Block-Copolymer Amphiphiles. *Nano Lett.* **2004**, *4*, 1055–1058.

(8) Neelakandan, P. P.; Pan, Z.; Hariharan, M.; Zheng, Y.; Welssman, H.; Rybtchinski, B.; Lewis, F. D. Hydrophobic self-Assembly of a Perylenediimide-Linked DNA Dumbbell into Supramolecular Polymers. *J. Am. Chem. Soc.* **2010**, *132*, 15808–15813.

(9) Carneiro, K. M. M.; Aldaye, A. F.; Sleiman, F. H. Long-Range Assembly of DNA into Nanofibers and Highly Ordered Networks Using a Block Copolymer Approach. *J. Am. Chem. Soc.* **2010**, *132*, 679–685.

(10) Carneiro, K. M. M.; Hamblin, G. D.; D., H. K.; Fakhoury, J.; Nayak, M. K.; Rizis, G.; McLaughlin, C. K.; Bazzi, H. S.; Sleiman, F. H. Stimuli-Responsive Organization of Block Copolymers on DNA Nanotubes. *Chem. Sci.* **2012**, *3*, 1980–1986.

(11) Edwardson, T. G. W.; Carneiro, K. M. M.; McLaughlin, C. K.; Serpell, C. J.; Sleiman, H. F. Site-Specific Positioning of Dendritic Alkyl Chains on DNA Cages Enables their Geometry-Dependent Self-Assembly. *Nat. Chem.* **2013**, *5*, 868–875.

(12) Wilks, T. R.; Bath, J.; de Vries, J. W.; Raymond, J. E.; Herrmann, A.; Turberfield, A. J.; O'Reilly, R. K. "Giant Surfactants" Created by the Fast and Efficient Functionalization of a DNA Tetrahedron with a Temperature-Responsive Polymer. *ACS Nano* **2013**, *7*, 8561–8572.

(13) Serpell, J. C.; Edwardson, W. G. T.; Chidchob, P.; Carneiro, M. M. K.; Sleiman, F. H. Precision Polymers and 3D DNA Nanostructures: Emergent Assemblies from New Parameter Space. *J. Am. Chem. Soc.* **2014**, *134*, 4280–4286.

(14) Nie, Z.; Fava, D.; Kumacheva, E.; Zou, S.; Walker, G. C.; Rubinstein, M. Self-Assembly of Metal-Polymer Analogues of Amphiphilic Triblock Copolymers. *Nature* **2007**, *6*, 609–614.

(15) Onsager, L. The Effects of Shape on the Interaction of Colloidal Particles. *Ann. N.Y. Acad. Sci.* **1949**, *51*, 627–659.

(16) Strzelecka, T. E.; Rill, R. L. Solid-state 31P NMR Studies of DNA Liquid Crystalline Phases. The Isotropic to Cholesteric Transition. *J. Am. Chem. Soc.* **1987**, *109*, 4513–4518.

(17) Livolant, F.; Leforestier, A. Condensed Phases of DNA : Structures and Phase Transitions. *Prog. Polym. Sci.* **1996**, *21*, 1115–1164.

(18) Chen, J. T.; Thomas, E. L.; Ober, C. K.; Mao, G. P. Self-Assembled Smectic Phases in Rod-Coil Block Copolymers. *Science* **1996**, *273*, 343–346.

(19) Sing, C. E.; Zwanikken, J. W.; de la Cruz, M. O. Electrostatic Control of Block Copolymer Morphology. *Nat. Mater.* **2014**, *13*, 694–698.

(20) Zhang, J.; Lettinga, M. P.; Dhont, J. K. G.; Stiakakis, E. Direct Visualization of Conformation and Dense Packing of DNA-Based Soft Colloids. *Phys. Rev. Lett* **2014**, *113*, 268303.

(21) Zhang, Z.; Horsch, M. A.; Lamm, M. H.; Glotzer, S. C. Tethered Nano Building Blocks: Toward a Conceptual Framework for Nanoparticle Self-Assembly. *Nano Lett.* **2003**, *3*, 1341–1346.

(22) Agard, N. J.; Prescher, J. A.; Bertozzi, C. R. A Strain-Promoted 3+2 Azide-Alkyne Cycloaddition for Covalent Modification of Biomolecules in Living Systems. *J. Am. Chem. Soc.* **2004**, *126*, 15046–15047.

(23) Zhang, Z.; Glotzer, S. C. Self-Assembly of Patchy Particles. *Nano Lett.* **2004**, *4*, 1407–1413.

(24) Yi, G.-R.; Pine, D. J.; Sacanna, S. Recent Progress on Patchy Colloids and their Self-Assembly. *J. Phys.: Condens. Matter* **2013**, *25*, 193101–12.

(25) Salamonczyk, M.; Zhang, J.; Portale, G.; Zhu, C.; Kentzinger, E.; Gleeson, J. T.; Jakli, A.; Michele, C. D.; Dhont, J. K. G.; Sprunt, S.; Stiakakis, E. Smectic Phase in Suspensions of Gapped DNA Duplexes. *Nat. Commun.* **2016**, *7*, 13358.

(26) Livolant, F.; Levelut, A. M.; Doucet, J.; Benoit, J. P. The Highly Concentrated Liquid-Crystalline Phase of DNA is Columnar Hexagonal. *Nature* **1989**, *339*, 724–726.

(27) Durand, D.; Doucet, J.; Livolant, F. A Study of the Structure of Highly Concentrated Phases of DNA by X-ray Diffraction. *J. Phys. II* **1992**, *2*, 1769–1783.

(28) Hajduk, D. A.; Harper, P. E.; Gruner, S. M.; Honeker, C. C.; Kim, G.; Thomas, E. L.; Fetters, L. J. The Gyroid: A New Equilibrium Morphology in Weakly Segregated Diblock Copolymers. *Macromolecules* **1994**, *27*, 4063–4075.

(29) Winey, K. I.; Thomas, E. L.; Fetters, L. J. The Ordered Bicontinuous Double-Diamond Morphology in Diblock Copolymer/Homopolymer Blends Macromolecules. *Macromolecules* **1992**, *25*, 422– 428.

(30) Chu, C. Y.; Lin, W. F.; Tsai, J. C.; Lai, C. S.; Lo, C. S.; Chen, H. L.; Hashimoto, H. L. Order–Order Transition between Equilibrium Ordered Bicontinuous Nanostructures of Double Diamond and Double Gyroid in Stereoregular Block Copolymer Macromolecules. *Macromolecules* **2012**, *45*, 2471–2477.

(31) Chu, C. Y.; Jiang, X.; Jinnai, H.; Pei, R. Y.; Lin, W. F.; Tsai, J. C.; Chen, H. L. Real-Space evidence of the Equilibrium Ordered Bicontinuous Double Diamond Structure of a Diblock Copolymer. *Soft Matter* **2015**, *11*, 1871–6.

(32) Hajduk, D. A.; Harper, P. E.; Gruner, S. M.; Honeker, C. C.; Thomas, E. L.; Fetters, L. J. A Reevaluation of Bicontinuous Cubic Phases in Starblock Copolymers. *Macromolecules* **1995**, *28*, 2570–2573.

(33) Meuler, A. J.; Hillmyer, M. A.; Bates, F. S. Ordered Network Mesostructures in Block Polymer Materials. *Macromolecules* **2009**, *42*, 7221–7250.

(34) Cherstvy, A. G. DNA Cholesteric Phases: The Role of DNA Molecular Chirality

and DNA–DNA Electrostatic Interactions. *J. Phys. Chem. B* **2008**, *130*, 184106–184108.

(35) Horsch, M. A.; Zhang, Z.; Glotzer, S. H. Self-Assembly of Polymer-Tethered Nanorods. *Phys. Rev. Lett* **2005**, *95*, 056105–1.

(36) Myung, J. S.; Taslimi, F.; Winkler, R. G.; Gompper, G. Self-Organized Structures of Attractive End-Functionalized Semiflexible Polymer Suspensions. *Macromolecules* **2014**, *47*, 4118–4125.

(37) Schwarz, U. S.; Gompper, G. Stability of Inverse Bicontinuous Cubic Phases in Lipid-Water Mixtures. *Phys. Rev. Lett.* **2000**, *85*, 1472 – 1475.

(38) Nakata, M.; Zanchetta, G.; Chapman, B. D.; Jones, C. D.; Cros, J. O.; Pindak, R.; Bellini, T.; Clark, N. A. End-to-End Stacking and Liquid Crystal Condensation of 6 to 20 Base Pair DNA duplexes. *Science* **2007**, *318*, 1276–1279.

(39) Kilchherr, F.; Wachauf, C.; Pelz, B.; Rief, M.; Zacharias, M.; Dietz, H. Single-Molecule Dissection of Stacking Forces in DNA. *Science* **2016**, *353*, aaf5508–9.

(40) Mezzenga, R.; Meyer, C.; Servais, C.; Romoscanu, A. I.; Sagalowicz, L.; Hayward, R. C. Shear Rheology of Lyotropic Liquid Crystals: A Case Study. *Langmuir* **2005**, *21*, 3322–3333.

(41) Alexandridis, P.; Olsson, U.; Lindman, B. A Record Nine Different Phases (Four Cubic, Two Hexagonal, and One Lamellar Lyotropic Liquid Crystalline and Two Micellar Solutions) in a Ternary Isothermal System of an Amphiphilic Block Copolymer and Selective Solvents (Water and Oil). *Langmuir* **1998**, *14*, 2627–2638.

(42) Su, Z.; Zhang, R.; Yan, X.; Guo, Q.; Huang, J.; Shan, W.; Liu, Y.; Liu, T.; Huang, M.; Cheng, S. Z. The Role of Architectural Engineering in Macromolecular Self-Assemblies *via* Non-Covalent Interactions: A Molecular LEGO Approach. *Prog. Polym. Sci.* **2020**, *103*, 101230.

(43) Jones, M. R.; Seeman, N. C.; Mirkin, C. A. Programmable Materials and the Nature of the DNA Bond. *Science* **2015**, *347*, 1260901–11.

(44) Seeman, N. C.; Sleiman, H. F. DNA Nanotechnology. *Nat. Rev. Mater.* **2017**, *3*, 17068.

(45) Duguet, E.; Hubert, C.; Chomette, C.; Perro, A.; Ravaine, S. Patchy Colloidal Particles for Programmed Self-Assembly. *C. R. Chim.* **2016**, *19*, 173–182.

(46) Dai, W.; Hsu, C. W.; Sciortino, F.; Starr, F. W. Valency Dependence of Polymorphism and Polyamorphism in DNA-Functionalized Nanoparticles. *Langmuir* **2010**, *26*, 3601–3608.

(47) Wang, Y.; Wang, Y.; Breed, D. R.; Manoharan, V. N.; Feng, L.; Hollingsworth, A. D.; Weck, M.; Pine, D. J. Colloids with Valence and Specific Directional Bonding. *Nature* **2012**, *491*, 51–56.

(48) Tian, Y.; Wang, T.; Liu, W.; Xin, H. L.; Li, H.; Ke, Y.; M., S. W.; Gang, O. Prescribed Nanoparticle Cluster Architectures and Low-Dimensional Arrays Built using Octahedral DNA Origami Frames. *Nat. Nanotechnol.* **2015**, *10*, 637–644.

(49) Chen, G.; Gibson, K. J.; Liu, D.; Rees, H. C.; Lee, J.-H.; Xia, W.; Lin, R.; Xin, H. L.; Gang, O.; Weizmann, Y. Regioselective Surface Encoding of Nanoparticles for Programmable Self-Assembly. *Nat. Mater.* **2019**, *18*, 169–174.

(50) Damasceno, P. F.; Engel, M.; Glotzer, S. C. Predictive Self-Assembly of Polyhedra into Complex Structures. *Science* **2012**, *337*, 453–457.

(51) van Anders, G.; Ahmed, N.; Smith, R.; Engel, M.; Glotzer, S. Entropically Patchy Particles: Engineering Valence through Shape Entropy. *ACS Nano* **2014**, *8*, 931–940.

(52) Pinheiro, A. V.; Han, D.; Shih, W. M.; Yan, H. Challenges and Opportunities for Structural DNA Nanotechnology. *Nat. Nanotechnol.* **2011**, *6*, 763–772.

(53) Matsukuma, D.; Yamamoto, K.; Aoyagi, T. Stimuli-Responsive Properties of N-Isopropylacrylamide-Based Ultrathin Hydrogel films Prepared by Photo-Cross-Linking. *Langmuir* **2006**, *22*, 5911–5915.

(54) Beines, P. W.; Klosterkamp, I.; Menges, B.; Jonas, U.; Knoll, W. Responsive Thin Hyrdogel Layers from Photo-Cross-Linkable Poly(N-isopropylacrylamide) Tetrapolymers. *Langmuir* **2007**, *92*, 6840–6846.

(55) Ho, K. M.; Chan, C. T.; Soukoulis, C. M. Existence of a Photonic Gap in Periodic Dielectric Structures. *Phys. Rev. Lett.* **1990**, *65*, 3152.

(56) Maldovan, M.; Urbas, A. M.; Yufa, N.; Carter, W. C.; Thomas, E. L. Photonic Properties of Bicontinuous Cubic Microphases. *Phys. Rev. B* **2002**, *65*, 165123.

(57) Maldovan, M.; Thomas, E. L. Diamond-Structured Photonic Crystals. *Nat. Mater.* **2004**, *3*, 593–600.

(58) Liu, W.; Tagawa, M.; Xin, H. L.; Wang, T.; Emamy, H.; Li, H.; Yager, K. G.; Starr, F. W.; Tkachenko, A. V.; Gang, O. Diamond Family of Nanoparticle Superlattices. *Science* **2016**, *351*, 582–586.

(59) Tan, S. J.; Campolongo, M. J.; Luo, D.; Cheng, W. Building Plasmonic Nanostructures with DNA. *Nat. Nanotechnol.* **2011**, *1*, 995.

(60) Nunes, S. P. Block Copolymer membranes for Aqueous Solution Applications. *Macromolecules* **2016**, *49*, 2905–2916.

(61) Bras, W. Recent Experiments on a Small-angle/Wide-Angle X-Ray Scattering Beam Line at the ESRF. *J. Appl. Crystallogr.* **2003**, *36*, 791–794.

(62) Kentzinger, E.; Krutyeva, M.; Rücker, U. GALAXI: Gallium Anode Low-Angle X-Ray Instrument. *Journal of large-scale research facilities* **2016**, *2*, A61.

Graphical TOC Entry